NATIONAL ADVISORY COMMITTEE FOR AERONAUTICS

TECHNICAL NOTE 2884

CALCULATION AND MEASUREMENT OF NORMAL MODES OF VIBRATION OF AN ALUMINUM-ALLOY BOX BEAM WITH AND WITHOUT LARGE DISCONTINUITIES

By Frank C. Smith and Darnley M. Howard

National Bureau of Standards

Washington

January 1953

1R

NATIONAL ADVISORY COMMITTEE FOR AERONAUTICS

TECHNICAL NOTE 2884

CALCULATION AND MEASUREMENT OF NORMAL MODES OF VIBRATION OF AN ALUMINUM-ALLOY BOX BEAM WITH AND WITHOUT LARGE DISCONTINUITIES

By Frank C. Smith and Darnley M. Howard

SUMMARY

The lowest normal modes of vibration of three aluminum-alloy box beams were calculated using a matrix iteration method. For these calculations the actual structures were idealized to a system of mass points interconnected by massless springs. The lowest normal modes of these beams were measured experimentally and compared with those calculated. This comparison indicates that the mode shapes and natural frequencies for structures of this type may be adequately calculated using this method. The experimental measurements were limited at the higher frequencies by local vibrations of small elements of the beams.

INTRODUCTION

A knowledge of the dynamic characteristics of modern aircraft structures is becoming increasingly important as the size and speed of aircraft continue to increase. High stresses can result from the dynamic response of an aircraft structure to landing impact forces, taxiing forces, or gust loads. In analyzing the dynamic response of such a structure to transient external forces the properties of the normal modes of the structure are widely used. An example of such use, in the case of the landing loads problem, is given in reference 1.

The calculation of the normal modes of a structure requires a knowledge of its mass distribution and its elastic characteristics. For geometrically simple structures, such as straight beams of uniform section, the elastic properties and the mass distribution may be expressed analytically and the normal modes easily calculated. However, practical structures, such as aircraft wings, usually have mass distributions not expressible in mathematical terms and elastic characteristics which are difficult to determine. Such a structure must be replaced by a simplified idealized structure to render it suitable for mathematical treatment. The more the real structure is simplified, the less laborious the analysis becomes, but the results of the analysis also become less accurate.

The present paper gives the results of calculations and tests made to determine the vibration characteristics of three reasonably complex structures whose design is generally similar to that used in aircraft. The results of the calculations of the lower modes of three built-up aluminum-alloy box beams, with and without large discontinuities, having large concentrated masses at their centers are compared with the results of vibration tests made on these beams.

The investigation was divided into three parts:

(1) The calculation and measurement of the lower modes of a beam with a D-nose and a large concentrated mass at its center

(2) The calculation and measurement of the lower modes of the same beam used in part (1) except that large cutouts were made in one of its cover sheets

(3) The calculation and measurement of the lower modes of the specimen used in part (2) except that the D-nose was removed

This work was done at the National Bureau of Standards and has been made available to the National Advisory Committee for Aeronautics for publication because of its general iterest.

The authors wish to express their appreciation to the staff of the Engineering Mechanics Section of the National Bureau of Standards for their assistance on this work. Particular thanks go to Mr. Samuel Levy for his help on the theoretical aspects of the problem and to Mr. A. E. McPherson, who designed the specimens and advised on the experimental methods used.

The authors also express their appreciation to the sponsors of this investigation, the Office of Naval Research, Department of the Navy, for releasing this work for publication.

SPECIMENS

Three specimens were used in the investigation. Specimen 1, used for the first part of the work, is shown in figure 1. Specimen 2, used for the second part of the work, was the same specimen, except that large cutouts were made in one of its cover sheets between the second and third bulkheads to each side of its spanwise center line. Specimen 3, used for the last part of the program, was the same as specimen 2 except that the D-nose was removed.

The basic specimen consisted of two built-up box beams fastened together with a heavy steel joint. Each beam was fabricated from 75S-T6 aluminum-alloy sheet and extruded angles. All rivets were $\frac{1}{8}$- inch diameter and made from A17S-T3 aluminum alloy. Static tests (references 2, 3, and 4) showed that for moderate loads the steel joint was elastic but that the flexibility of the joint was not negligible. The calculations of the section properties of the specimens were based on measured rather than nominal dimensions. As a check on these calculations the weight of specimen 1 was calculated as 350.1 pounds, using nominal densities for the aluminum and steel. The specimen was then weighed and found to weigh 359.5 pounds. It was felt that most of the error in calculating the weight of specimen 1 occurred in calculating the weight of the steel joint.

CALCULATION OF NORMAL MODES

General

The fundamental quantities necessary for the calculation of the normal modes of a structure are its elastic characteristics and its mass distribution. The mass distribution may be calculated from the dimensions of the structure and the densities of the materials from which the structure is fabricated. The elastic characteristics may be determined either from deflection measurements under static external loads or from theoretical calculations.

For the specimens used for these tests the mass distributions were calculated from measured dimensions and nominal densities. The elastic characteristics of the specimens were determined from theoretical considerations and from direct measurement (references 2, 3, and 4). The mode shapes and natural frequencies were calculated from these quantities using the theory given in reference 5.

In the case of aircraft wings, a usual assumption made in deflection calculations is that the wing is built into an infinitely rigid root. It will be shown later that some flexibility of the root can exist without seriously affecting the shapes of the calculated normal modes.

Idealized Specimens

For the purpose of calculating the normal modes, the actual specimens were replaced by idealized structures consisting of discrete mass points interconnected with massless springs as described in appendix II

of reference 5. The location and magnitude of these masses replacing each specimen were determined in the following manner.

It was decided to replace one-half of each actual structure with 14 coplanar masses arranged in pairs along the bulkhead center lines, a, b,. . . g (fig. 2). Seven of the mass points were assumed to lie along the center line of the rear shear web at the bulkheads, points 2, 4,. . . 14 (fig. 2). The magnitudes of all the masses and the z-coordinates of masses 1, 3,. . . 13, (y = 0 for these masses) were determined as follows: The semispecimen was considered divided into six free-bodies A, B,. . . F (fig. 2) by passing planes through the specimen as shown. Each free-body was considered resting on knife edges located at the bulkhead center lines, a, b,. . . g (fig. 2). The proportion of the mass of each free-body considered lying along these center lines was calculated from equilibrium considerations.

The total mass of the structure considered lying along any bulkhead center line was then obtained by adding the contributions of mass of the free-bodies adjacent to the center line in question to the mass of the bulkhead. The first moment and the moment of inertia about the x-axis (fig. 2) for each free-body A, B,. . . F were calculated and proportioned at the bulkhead center lines a, b,. . . g in direct proportion to the mass contributions of each free-body to the bulkhead center line. The magnitudes of all the masses and the z-coordinates, of the masses 1, 3,. . . 13, were calculated from

$$\left.\begin{aligned} Z_r &= I_n/Q_n \\ m_r &= Q_n/Z_r \\ m_s &= M_n - m_r \end{aligned}\right\} \qquad (1)$$

where

Z_r z-coordinate of rth mass, where r = 1, 3,. . . 13 (fig. 2)

I_n total moment of inertia contributed by adjacent free-bodies and included bulkhead to nth bulkhead line

Q_n total first moment contributed by adjacent free-bodies and included bulkhead to the nth bulkhead line

m_r magnitude of rth mass, where r = 1, 3,. . . 13 (fig. 2)

M_n total mass contributed by adjacent free-bodies and included bulkhead to nth bulkhead line

m_s magnitude of sth mass, where $s = 2, 4, \ldots 14$ (fig. 2)

The use of equation (1) resulted in a substitute discrete mass distribution whose mass, first moment, and moment of inertia about the x-axis were the same as those of the original specimen.

Tables 1, 2, and 3 give the magnitudes and locations of the mass points replacing the actual specimens.

The elastic characteristics of the specimens discussed here were defined in terms of their influence coefficients. An influence coefficient between two points is defined here as the deflection of one point in the y-direction (fig. 2) for a unit load in the y-direction at the other point when the center of the specimen is clamped. References 2 to 4 give measured influence coefficients, as well as those calculated from the theory given in reference 5, at 12 points corresponding to the intersections of the front and rear spars with the bulkheads. For use in calculating the mode shapes it was necessary to compute the influence coefficients at the mass-point locations, $3, 4, \ldots 14$, in figure 2 (those at points 1 and 2 are zero by definition). This was done by assuming the bulkheads remained rigid in their planes during small deflections and rotations and then interpolating from the known influence coefficients at the intersections of the front and rear spars with the bulkheads. The computed and measured influence coefficients thus obtained for specimen 1 at the mass-point locations are shown in tables 4 and 5, respectively. Tables 6 and 7, respectively, give measured values for specimens 2 and 3.

The theoretical influence coefficients for specimen 1 are calculated in reference 2 with the assumption that the steel joint at the center of the specimen was infinitely rigid, whereas the measured influence coefficients for this and the other specimens contain displacement components due to rotation and warping of the root. Comparison of tables 4 and 5 shows that this effect is not negligible.

Calculation of Mode Shapes and Natural Frequencies of Idealized Structures

The mode shapes and natural frequencies are calculated from the equations given in reference 5. Let $y_1, y_2, \ldots y_{14}$, be the displacements in the y-direction (fig. 2) of the mass points $m_1, m_2, \ldots m_{14}$

of a body free from externally applied forces. Then the displacement of any point m is given by:

$$y_m = -\sum_{n=1x}^{n=14} \delta_{m,n} m_n \ddot{y}_n + \lambda + \theta x_n + \alpha z_n \qquad (m = 1, 2, \ldots 14) \qquad (2)$$

where

$\delta_{m,n}$ deflection of structure at point m for a unit load applied at point n, with root clamped, (i.e., an influence coefficient)

λ displacement of root (x = y = z = 0) in y-direction

θ angle of rotation of root about z-axis

α angle of rotation of root about x-axis

$\ddot{y}_n$ acceleration in y-direction of nth mass

If it is assumed that the masses of the idealized structures are oscillating in simple harmonic motion:

$$\left.\begin{aligned} y_m &= a_m \sin \omega t \\ \lambda &= \lambda_{max} \sin \omega t \\ &\cdots\cdots \end{aligned}\right\} \qquad (3)$$

where

a_m maximum displacement of mth mass, inches

λ_{max} maximum displacement of root, inches

ω circular frequency of vibration, radians per second

t time, seconds

Substituting into equation (2) and dividing the resultant equations by $-\omega^2 \sin \omega t$ there is obtained:

$$\frac{1}{\omega^2}\left(a_m - \lambda_{max} - \theta_{max}x_m - \alpha_{max}z_m\right) = \sum_{n=1}^{n=14} \delta_{m,n}m_n a_n$$

$$(m = 1, 2, \ldots 14) \qquad (4)$$

In order to solve equations (4) a matrix composed of the masses and the influence coefficients is iterated as shown:

$$\begin{bmatrix} \delta_{1,1}m_1 + \delta_{1,2}m_2 + \delta_{1,3}m_3 \ldots \delta_{1,14}m_{14} \\ \delta_{2,1}m_1 + \delta_{2,2}m_2 + \delta_{2,3}m_3 \ldots \delta_{2,14}m_{14} \\ \delta_{3,1}m_1 + \delta_{3,2}m_2 + \delta_{3,3}m_3 \ldots \delta_{3,14}m_{14} \\ \vdots \\ \delta_{14,1}m_1 + \delta_{14,2}m_2 + \delta_{14,3}m_3 \ldots \delta_{14,14}m_{14} \end{bmatrix} \begin{bmatrix} a_1' \\ a_2' \\ a_3' \\ \vdots \\ a_{14}' \end{bmatrix} =$$

$$\frac{1}{(\omega'')^2}\begin{bmatrix} a_1'' - \lambda_{max}'' - \theta_{max}''x - \alpha_{max}''z \\ a_2'' - \lambda_{max}'' - \theta_{max}''x - \alpha_{max}''z \\ a_3'' - \lambda_{max}'' - \theta_{max}''x - \alpha_{max}''z \\ \vdots \\ a_{14}'' - \lambda_{max}'' - \theta_{max}''x - \alpha_{max}''z \end{bmatrix} \qquad (5)$$

where a_1', a_2', . . . a_{14}' are a first approximation of the mode shape and a_1'', a_2'', . . . a_{14}'' are a second approximation.

To determine λ_{max}'', θ_{max}'', and α_{max}'' the sums A, B, and C are computed from equations (4) as follows:

$$\left.\begin{aligned}
\sum_{1}^{14} m_m\left(a_m'' - \lambda_{max}'' - \theta_{max}'' x - \alpha_{max}'' z_m\right)\frac{1}{(\omega'')^2} &= \sum_{1}^{14} m_m \sum_{n=1}^{n=14} \delta_{m,n} m_n a_n' = A \\
\sum_{1}^{14} m_m x\left(a_m'' - \lambda_{max}'' - \theta_{max}'' x - \alpha_{max}'' z\right)\frac{1}{(\omega'')^2} &= \sum_{1}^{14} m_m x_m \sum_{n=1}^{n=14} \delta_{m,n} m_n a_n' = B \\
\sum_{1}^{14} m_m z\left(a_m'' - \lambda_{max}'' - \theta_{max}'' x - \alpha_{max}'' z\right)\frac{1}{(\omega'')^2} &= \sum_{1}^{14} m_m z_m \sum_{n=1}^{n=14} \delta_{m,n} m_n a_n' = C
\end{aligned}\right\} \quad (6)$$

By making use of the condition that the specimen is not accelerated as a rigid body:

$$\left.\begin{aligned}
\sum_{\text{body}} m_n a_n'' &= 0 \\
\sum_{\text{body}} m_n x_n a_n'' &= 0 \\
\sum_{\text{body}} m_n z_n a_n'' &= 0
\end{aligned}\right\} \quad (7)$$

For symmetrical vibratory modes, the displacements a_n'' are the same on the right- and left-hand portions of the specimen with the result that equations (6) reduce to

$$\left.\begin{aligned} \sum_{n=1}^{14} m_n a_n'' &= 0 \\ \sum_{n=1}^{14} m_n z_n a_n'' &= 0 \end{aligned}\right\} \tag{7a}$$

For antisymmetrical vibratory modes, the displacements a_n'' are of opposite signs for the two halves of the specimen with the result that equations (6) reduce to

$$\sum_{n=1}^{14} m_n x_n a_n'' = 0 \tag{7b}$$

For symmetric modes, taking $\theta''/(\omega'')^2$ as zero and substituting equations (7a) into the first and third of equations (6)

$$\left.\begin{aligned} -\frac{\lambda_{max}''}{(\omega'')^2}\sum_{m=1}^{14} m_m - \frac{\alpha_{max}''}{(\omega'')^2}\sum_{m=1}^{14} m_m z_m &= A \\ -\frac{\lambda_{max}''}{(\omega'')^2}\sum_{m=1}^{14} m_m z_m - \frac{\alpha_{max}''}{(\omega'')^2}\sum_{m=1}^{14} m_m z_m^2 &= C \\ \left(\frac{\theta''}{(\omega'')^2} = 0\right) & \end{aligned}\right\} \tag{8a}$$

For antisymmetric modes, taking $\lambda''/(\omega'')^2$ and $\alpha''/(\omega'')^2$ as zero and substituting equation (7b) into the second of equations (6)

$$-\frac{\theta''_{max}}{(\omega'')^2}\sum_{m=1}^{14} m_m x_m^2 = B$$

$$\left(\frac{\lambda''}{(\omega'')^2} = \frac{\alpha''}{(\omega'')^2} = 0\right) \qquad (8b)$$

The summations in equations (8) are computed from the mass distribution and geometry of the specimen. Knowing these and A, B, and C, $\lambda''/(\omega'')^2$, $\theta''/(\omega'')^2$, and $\alpha''/(\omega'')^2$ can be evaluated by solving equations (8a) for symmetric modes and (8b) for antisymmetric modes. By combining the results of equations (5) with the solution of equations (8) $a_m''/(\omega'')^2$ is given:

$$\frac{a_m''}{(\omega'')^2} = \frac{1}{(\omega'')^2}\left(a_m'' - \lambda''_{max} - \theta''_{max}x_m - \alpha''_{max}z_m\right) + \frac{\lambda_{max}}{(\omega'')^2} + \frac{\theta_{max}x}{(\omega'')^2} + \frac{\alpha_{max}z}{(\omega'')^2} \qquad (9)$$

The new approximate mode shape is normalized for the next iteration by forming the ratios

$$\frac{a_m''/(\omega'')^2}{a_{14}''/(\omega'')^2}$$

The approximate value of ω^2 is taken as

$$\frac{a'_{14}}{a_{14}''/(\omega'')^2}$$

The iteration procedure used in solving equations (4) causes the solution to converge to the lowest mode. These equations may be solved for higher modes if the modes with lower frequencies than the assumed mode are "swept" out. This procedure, based on the fact that the solutions for equations (4) are orthogonal, is derived in reference 6. Equations (4) were set up for four cases:

(1) Specimen 1, using the calculated influence coefficients given in table 4

(2) Specimen 1, using the measured influence coefficients given in table 5

(3) Specimen 2, using the measured influence coefficients given in table 6

(4) Specimen 3, using the measured influence coefficients given in table 7

The four sets of equations (4) were solved for the following modes by the matrix iteration process given in reference 5:

(1) Specimen 1 (calculated and measured influence coefficients): Three lowest natural frequencies and associated mode shapes

(2) Specimen 2 (measured influence coefficients): Four lowest natural frequencies and associated mode shapes

(3) Specimen 3 (measured influence coefficients): Three lowest natural frequencies and associated mode shapes

The displacements of the masses obtained from the iteration were interpolated to obtain a set of displacements at the intersections of the bulkheads with the front and rear spars. These displacements were normalized by dividing them by the displacement at the intersection of the end bulkhead with the front spar. The resulting mode shapes for those cases where experimental results were obtained are shown in figures 3 to 6 and their natural frequencies are given in table 8.

Figures 3(a), 3(b), and 3(c) show that although there was a serious discrepancy between the calculated and measured influence coefficients for specimen 1, due, probably, to the elastic rotation and warping of the steel joint at the center of the specimen, the mode shapes of the two cases agree fairly well, whereas the natural frequencies calculated from the theoretical influence coefficients are 4 to 15 percent higher than those calculated from the measured influence coefficients.

EXPERIMENTAL CONFIRMATION OF THEORY

General

All of the specimens were tested in the same manner. Figure 7 shows a typical test arrangement with specimen 2. The specimen was suspended from the cantilevered channel A by four soft helical springs B (fig. 7). The specimen was excited in a direction normal to its width by a loudspeaker-type shaker motor C (fig. 7). The stationary field coils of this motor were excited by about 6 amperes of 110-volt direct current. The reciprocating armature, which was connected to the steel joint of the specimen by a $\frac{1}{4}$- inch-square aluminum-alloy dynamometer, was excited by an amplified oscillator signal. The dynamometer had a low flexural stiffness, so the restraint to the specimens offered by the springs and dynamometer, except in the axial direction of the dynamometer, was low. The restraint in the axial direction of the dynamometer was made negligible by adjusting the frequency until the ratio of specimen amplitude to dynamometer force was a maximum.

The dynamometer was equipped with four $\frac{1}{4}$- inch gage length SR-4 wire strain gages. These gages were connected to a modified SR-4 indicator and a cathode-ray oscilloscope in such a manner that the steady-state dynamic axial strain in the dynamometer could be measured to ±2 microinches.

The relative accelerations at selected locations along front and rear spars were measured with vacuum-tube accelerometers (reference 7). The output of these accelerometers was a single sinusoidal wave the amplitude of which could be accurately measured.

Determination of Natural Frequencies

An additional vacuum-tube accelerometer was attached to the tip P (fig. 7). The specimen was excited at various frequencies and the steady-state dynamic strain in the dynamometer together with the relative acceleration of the tip of the beam was measured. The specimen was assumed to be in resonance when the ratio of the relative acceleration at the tip of the specimen to the strain in the dynamometer (i.e., driving force) was a maximum. A resonance curve for each specimen was plotted during the frequency sweep tests and the maximums of the curve reexamined at small increments in the frequency, about 2 cycles per second, to determine those frequencies best representing the resonant frequencies. Figure 8 shows the resonance curves for the three specimens.

Determination of Normalized Mode Shapes

When the resonant frequencies for a specimen had been determined, the specimen was excited at resonance and the relative mode shape measured with vacuum-tube accelerometers. One accelerometer was left at Q (fig. 7). Other accelerometers were clamped at points every 6 inches along the front and rear spars. Measurements of the relative accelerations at location Q (fig. 7) and the point in question were made simultaneously. The acceleration of the point was then calculated relative to a unit acceleration at Q. In this manner normalized acceleration values were determined. At a fixed frequency of harmonic motion, the acceleration amplitude is proportional to the displacement amplitude; therefore, these normalized acceleration values represented the normalized displacement values of the measured points on the beam, or the shapes assumed by the pairs of angles when the specimen was at resonance. This may not be true when damping is present.

The following mode shapes were measured:

Specimen 1: Lowest three modes. Two sets of measurements were made of each mode shape.

Specimen 2: First, second, and fourth modes. Two sets of measurements were made of each mode shape. The first four modes were calculated, but the third mode, a torsion mode, was not excited experimentally with the force applied as was done in the test. By the time the computations were complete, the test arrangement had been dismantled and could not be repeated with a better point of force application.

Specimen 3: First and third modes. The second measured mode, again a torsion mode, was not excited to any extent.

Local deformations of the specimens between bulkheads were observed at a frequency of about 230 cycles per second. These deformations are not included in the theory, so it was not considered worth while to measure the mode shapes of any modes above about 230 cycles per second.

COMPARISON OF THEORY AND EXPERIMENT

Figures 4, 5, and 6 show the results of the tests superposed on the calculated mode shapes. Table 8 shows the comparison between calculated and measured natural frequencies for the three specimens.

It can be seen that the theory, which considers the mass concentrated at the bulkheads, can be used to predict the natural frequencies to within about 6 percent, provided flexibility at the root of the

specimen is taken into account, that is, that the influence coefficients of the structure are known accurately. Figure 3 shows that, using the influence coefficients calculated with the assumption of a rigid root, the errors in the natural frequencies range from 19 percent for the lowest frequency to 10 percent for the second natural frequency, although the errors in the mode shapes are reasonably small.

CONCLUDING REMARKS

The tests reported here indicate that the mode shapes and natural frequencies of the fundamental and several higher modes for a structure with and without large discontinuities may be adequately calculated by a matrix iteration method, assuming the mass of the structure concentrated at the bulkheads, provided that the elastic constants of the structure are accurately known. The presence of some flexibility in the root may produce large errors in the influence coefficients. Such flexibility does not result, however, in serious errors in the mode shapes, but does result in appreciable errors in the calculated natural frequencies.

The experimental measurement of response over a range of frequencies showed that at the higher frequencies there were appreciable local vibrations of small elements of the beam. No attempt was made to check these vibrations by making an analysis of the beam with a finer mass distribution, since it was felt that these local vibrations have no structural significance although they may be bothersome in the elements in which they occur.

National Bureau of Standards
Washington 25, D. C., April 16, 1952

REFERENCES

1. Biot, M. A., and Bisplinghoff, R. L.: Dynamic Loads on Airplane Structures during Landing. NACA ARR 4H10, 1944.

2. Weaver, Preston R., Kroll, Wilhelmina D., and Garland, William A.: Experimental Determination of Influence Coefficients for a Monocoque Structure. Prog. Rep. 1, NBS Lab. No. 6.4/1-209, NA onr 31-48, NR-035-200, NBS, Bur. Aero., and ONR, May 4, 1949.

3. Kroll, Wilhelmina D., Weaver, Preston R., and Garland, William A.: Influence Coefficients of a Single-Cell Monocoque Box Beam Having a Full Bay Cut-Out. Prog. Rep. 2, Lab. No. 6.4/1-209, NA onr 31-48, NR-035-200, NBS, Bur. Aero., and ONR, June 19, 1950.

4. Garland, William A., Kroll, Wilhelmina D., and Weaver, Preston R.: Influence Coefficients of a Two-Cell Monocoque Box Beam Having a Full Bay Cut-Out. Prog. Rep. 3, NBS Lab. No. 6.4/209, Proj. No. 3514, NA onr 31-48, (NR 035-200), NR 064-200, NBS, Bur. Aero., and ONR, Feb. 20, 1951.

5. Levy, Samuel: Computation of Influence Coefficients for Aircraft Structures with Discontinuities and Sweepback. Jour. Aero. Sci., vol. 14, no. 10, Oct. 1947, pp. 547-560.

6. Ramberg, Walter, and Levy, Sam: Calculation of Stresses and Natural Frequencies for a Rotating Propeller Blade Vibrating Flexurally. Jour. Res., Nat. Bur. Standards, Res. Paper RP1148, vol. 21, Nov. 1938, pp. 639-669.

7. Ramberg, Walter: The Measurement of Acceleration with a Vacuum Tube. Trans. A.I.E.E., vol. 66, Nov. 1947, pp. 735-740.

TABLE 1

LOCATION AND MAGNITUDES OF MASS POINTS[1]

REPLACING SPECIMEN 1

Point	Mass ($lb\text{-}sec^2/in.$)	Coordinates (in.)		
		x	y	z
1	0.1328	0	0	-10.55
2	.0835	0	0	0
3	.0920	8.75	0	-10.63
4	.0584	8.75	0	0
5	.00760	20.75	0	-12.23
6	.00562	20.75	0	0
7	.00760	32.75	0	-12.23
8	.00562	32.75	0	0
9	.00760	44.75	0	-12.23
10	.00562	44.75	0	0
11	.00753	56.75	0	-12.23
12	.00558	56.75	0	0
13	.00540	68.75	0	-12.10
14	.00372	68.75	0	0

[1]See fig. 2 for coordinate system.

TABLE 2

LOCATION AND MAGNITUDES OF MASS POINTS[1]

REPLACING SPECIMEN 2

Point	Mass ($lb\text{-}sec^2/in.$)	Coordinates (in.)		
		x	y	z
1	0.1328	0	0	-10.55
2	.0835	0	0	0
3	.0920	8.75	0	-10.63
4	.0584	8.75	0	0
5	.00705	20.75	0	-12.40
6	.00524	20.75	0	0
7	.00705	32.75	0	-12.40
8	.00524	32.75	0	0
9	.00760	44.75	0	-12.23
10	.00562	44.75	0	0
11	.00753	56.75	0	-12.23
12	.00558	56.75	0	0
13	.00540	68.75	0	-12.10
14	.00372	68.75	0	0

[1]See fig. 2 for coordinate system.

TABLE 3

LOCATION AND MAGNITUDES OF MASS POINTS[1]

REPLACING SPECIMEN 3

Point	Mass ($lb\text{-}sec^2/in.$)	Coordinates (in.)		
		x	y	z
1	0.1328	0	0	-10.55
2	.0835	0	0	0
3	.0913	8.75	0	-10.59
4	.0583	8.75	0	0
5	.00611	20.75	0	-11.69
6	.00530	20.75	0	0
7	.00611	32.75	0	-11.69
8	.00530	32.75	0	0
9	.00643	44.75	0	-11.58
10	.00548	44.75	0	0
11	.00637	56.75	0	-11.58
12	.00543	56.75	0	0
13	.00456	68.75	0	-11.41
14	.00370	68.75	0	0

[1]See fig. 2 for coordinate system.

TABLE 4

COMPUTED INFLUENCE COEFFICIENTS, SPECIMEN 1

Load at -	Deflection (in./lb) at - (1)													
	1	2	3	4	5	6	7	8	9	10	11	12	13	14
1	0	0	0	0	0	0	0	0	0	0	0	0	0	0
2	0	0	0	0	0	0	0	0	0	0	0	0	0	0
3	0	0	0	0	0	0	0	0	0	0	0	0	0	0
4	0	0	0	0	0	0	0	0	0	0	0	0	0	0
5	0	0	0	0	$\underline{7.65} \times 10^{-6}$	3.00×10^{-6}	9.74×10^{-6}	5.65×10^{-6}	12.38×10^{-6}	8.22×10^{-6}	14.91×10^{-6}	10.77×10^{-6}	17.46×10^{-6}	13.32×10^{-6}
6	0	0	0	0	3.00	$\underline{10.53}$	5.63	13.10	8.19	15.65	10.73	18.20	13.36	20.75
7	0	0	0	0	9.74	5.63	$\underline{25.49}$	15.84	35.44	26.02	45.59	36.19	55.78	46.36
8	0	0	0	0	5.65	13.10	15.84	$\underline{31.78}$	26.01	42.13	36.17	52.36	46.51	62.57
9	0	0	0	0	12.38	8.19	35.44	26.01	$\underline{63.89}$	48.81	86.59	71.66	109.51	94.52
10	0	0	0	0	8.22	15.65	26.02	42.13	48.81	$\underline{73.72}$	71.65	96.85	94.77	119.87
11	0	0	0	0	14.91	10.73	45.59	36.17	86.59	71.65	$\underline{132.92}$	112.19	173.57	152.71
12	0	0	0	0	10.77	18.20	36.19	52.36	71.66	96.85	112.19	$\underline{146.35}$	153.05	187.50
13	0	0	0	0	17.46	13.36	55.78	46.51	109.51	94.77	173.57	153.05	$\underline{243.12}$	215.95
14	0	0	0	0	13.32	20.75	46.36	62.57	94.52	119.87	152.71	187.50	215.95	$\underline{260.63}$

[1]Values represent calculated influence coefficients at mass points of idealized structure shown in fig. 2. Off-diagonal values have been averaged to agree with Maxwell's reciprocity theorem.

TABLE 5

MEASURED INFLUENCE COEFFICIENTS, SPECIMEN 1

Load at -	Deflection (in./lb) at - (1)													
	1	2	3	4	5	6	7	8	9	10	11	12	13	14
1	0	0	0	0	0	0	0	0	0	0	0	0	0	0
2	0	0	0	0	0	0	0	0	0	0	0	0	0	0
3	0	0	0	0	2.2×10^{-6}	1.1×10^{-6}	2.8×10^{-6}	1.5×10^{-6}	3.0×10^{-6}	2.0×10^{-6}	3.2×10^{-6}	2.3×10^{-6}	4.2×10^{-6}	2.9×10^{-6}
4	0	0	0	0	1.0	3.5	1.5	4.3	1.8	5.0	2.1	5.5	3.2	6.4
5	0	0	2.2×10^{-6}	1.0×10^{-6}	12.8	5.9	17.7	11.3	22.8	16.6	27.2	21.2	33.3	26.2
6	0	0	1.1	3.5	5.9	16.5	11.1	22.6	16.1	28.1	21.0	33.1	26.6	38.3
7	0	0	2.8	1.5	17.7	11.1	38.5	25.7	53.2	41.3	67.3	55.9	82.9	71.1
8	0	0	1.5	4.3	11.3	22.6	25.7	46.7	40.5	63.1	55.1	77.8	70.8	92.5
9	0	0	3.0	1.8	22.8	16.1	53.2	40.5	88.9	71.1	117.9	100.6	148.2	130.2
10	0	0	2.0	5.0	16.6	28.1	41.3	63.1	71.1	102.2	100.6	132.8	131.6	162.7
11	0	0	3.2	2.1	27.2	21.0	67.3	55.1	117.9	100.6	173.1	149.6	224.4	199.2
12	0	0	2.3	5.5	21.2	33.1	55.9	77.8	100.6	132.8	149.6	192.1	201.9	242.9
13	0	0	4.2	3.2	33.3	26.6	82.9	70.8	148.2	131.6	224.4	201.9	305.2	275.9
14	0	0	2.9	6.4	26.2	38.3	71.1	92.5	130.2	162.7	199.2	242.9	275.9	328.7

[1]Values correspond to influence coefficients at mass points of idealized structure shown in fig. 2. Off-diagonal values have been averaged to agree with Maxwell's reciprocity theorem.

TABLE 6

MEASURED INFLUENCE COEFFICIENTS, SPECIMEN 2

Load at -	Deflection (in./lb) at - (1)													
	1	2	3	4	5	6	7	8	9	10	11	12	13	14
1	0	0	0	0	0	0	0	0	0	0	0	0	0	0
2	0	0	0	0	0	0	0	0	0	0	0	0	0	0
3	0	0	0	0	2.85×10^{-6}	1.04×10^{-6}	3.60×10^{-6}	1.29×10^{-6}	3.55×10^{-6}	1.87×10^{-6}	4.35×10^{-6}	2.31×10^{-6}	4.80×10^{-6}	3.14×10^{-6}
4	0	0	0	0	1.03	1.78	1.83	1.98	1.82	2.445	2.84	2.885	3.07	3.595
5	0	0	2.85×10^{-6}	1.03×10^{-6}	16.55	5.65	22.60	11.03	28.35	16.05	34.15	21.21	38.98	26.98
6	0	0	1.04	1.78	5.65	12.57	11.11	17.97	16.16	22.525	21.70	27.875	26.76	33.26
7	0	0	3.60	1.83	22.60	11.11	50.30	24.04	68.30	39.79	84.73	55.79	100.73	72.40
8	0	0	1.29	1.98	11.03	17.97	24.04	40.59	39.84	55.71	55.88	73.655	71.62	89.595
9	0	0	3.55	1.82	28.35	16.16	68.30	39.84	111.20	71.15	145.28	104.08	178.18	138.81
10	0	0	1.87	2.445	16.05	22.525	39.79	55.71	71.15	96.53	104.31	128.545	136.57	161.12
11	0	0	4.35	2.84	34.15	21.70	84.73	55.88	145.28	104.31	211.90	159.16	265.83	218.21
12	0	0	2.31	2.885	21.21	27.875	55.79	73.655	104.08	128.545	159.16	190.45	213.26	246.44
13	0	0	4.80	3.07	38.98	26.76	100.73	71.62	178.18	136.57	265.83	213.26	358.45	297.95
14	0	0	3.14	3.595	26.98	33.26	72.40	89.595	138.81	161.12	218.21	246.44	297.95	338.09

[1]Values correspond to influence coefficients at mass points of idealized structure shown in fig. 2. Off-diagonal values have been averaged to agree with Maxwell's reciprocity theorem.

TABLE 7

MEASURED INFLUENCE COEFFICIENTS, SPECIMEN 3

Load at -	Deflection (in./lb) at - (1)												
	1	2	3	4	5	6	7	8	9	10	11	12	13	14
1	0	0	0	0	0	0	0	0	0	0	0	0	0	0
2	0	0	0	0	0	0	0	0	0	0	0	0	0	0
3	0	0	0	0	2.45×10^{-6}	1.16×10^{-6}	2.96×10^{-6}	1.47×10^{-6}	3.46×10^{-6}	2.11×10^{-6}	3.57×10^{-6}	2.55×10^{-6}	4.11×10^{-6}	3.30×10^{-6}
4	0	0	0	0	.96	3.10	1.55	3.50	2.16	3.70	2.28	4.40	3.16	6.30
5	0	0	2.45×10^{-6}	$.96 \times 10^{-6}$	15.97	6.20	22.96	11.07	28.76	16.44	34.32	21.16	39.63	27.53
6	0	0	1.16	3.10	6.20	17.70	11.41	25.00	16.97	31.30	22.08	36.65	28.07	42.05
7	0	0	2.96	1.55	22.96	11.41	51.68	23.71	70.34	39.61	87.03	56.37	103.64	73.42
8	0	0	1.47	3.50	11.07	25.00	23.71	54.40	40.47	74.05	56.94	91.25	74.79	108.35
9	0	0	3.46	2.16	28.76	16.97	70.34	40.47	114.16	73.77	149.77	108.09	184.71	144.02
10	0	0	2.11	3.70	16.44	31.30	39.61	74.05	73.77	121.20	107.70	157.30	144.08	192.90
11	0	0	3.57	2.28	34.32	22.08	87.03	56.94	149.77	107.70	215.85	166.10	275.66	224.74
12	0	0	2.55	4.40	21.16	36.65	56.37	91.25	108.09	157.30	166.10	225.40	226.62	285.05
13	0	0	4.11	3.16	39.63	28.07	103.64	74.79	184.71	144.08	275.66	226.62	375.22	314.53
14	0	0	3.30	6.30	27.53	42.05	73.42	108.35	144.02	192.90	224.74	285.05	314.53	382.70

[1]Values represent influence coefficients at mass points of idealized structure shown in fig. 2. Off-diagonal values have been averaged to agree with Maxwell's reciprocity theorem.

TABLE 8

COMPARISON OF CALCULATED AND MEASURED NATURAL FREQUENCIES OF SPECIMENS

Specimen	Natural frequency (cps)							
	First mode		Second mode		Third mode		Fourth mode	
	Measured	Calculated	Measured	Calculated	Measured	Calculated	Measured	Calculated
[a]1a	66	68.4	181	190.2	221	234.6	---	-----
[b]1b	66	78.4	181	198.1	221	252.5	---	-----
2	63	64.8	173	181.3	---	184.7	198	204.7
3	64	66.3	---	164.3	173	179.5	---	-----

[a]1a, calculated using measured influence coefficients.

[b]1b, calculated using theoretical influence coefficients.

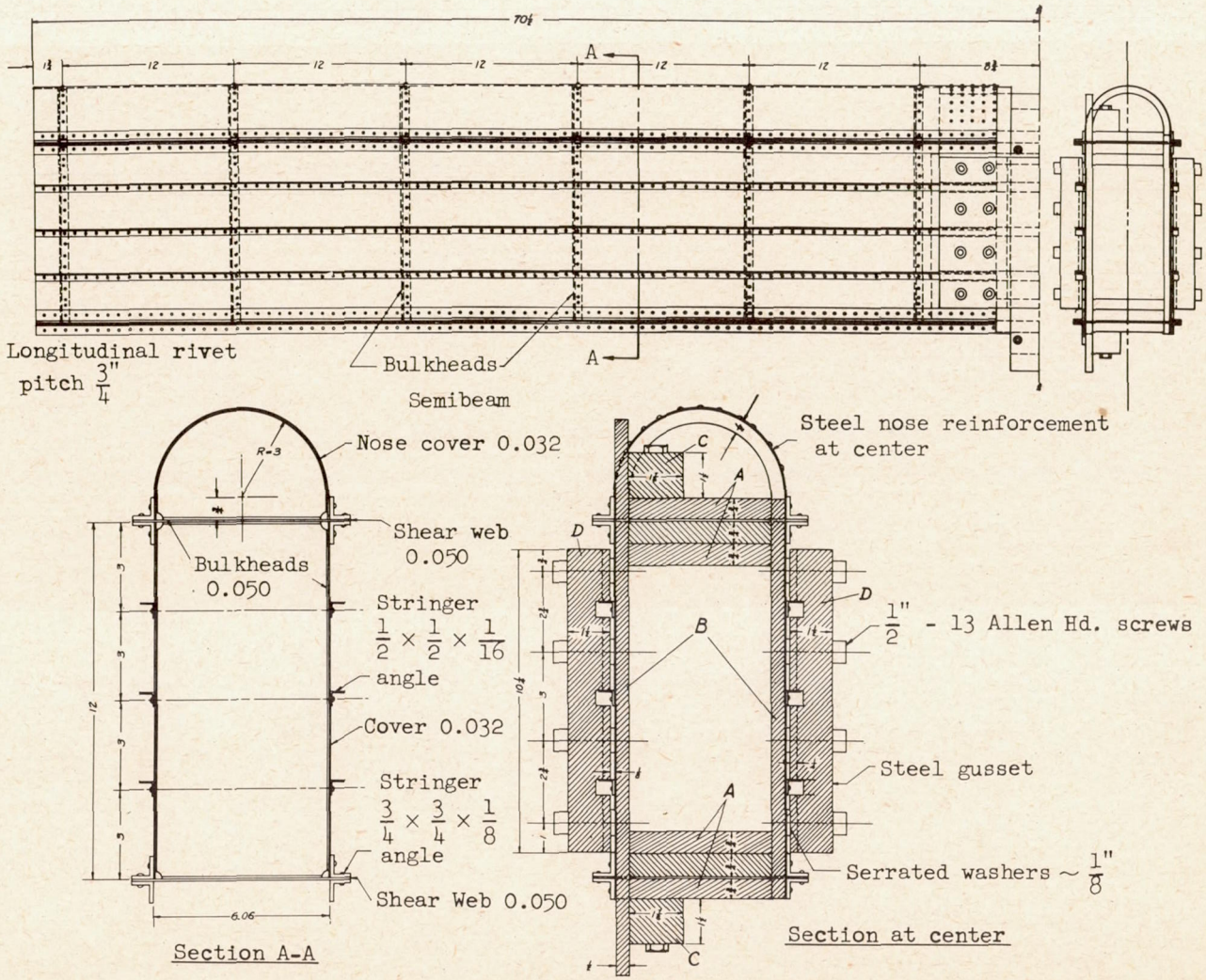

Figure 1.- Design of specimen. All dimensions in inches. All rivets A17S-T3 brazier head.

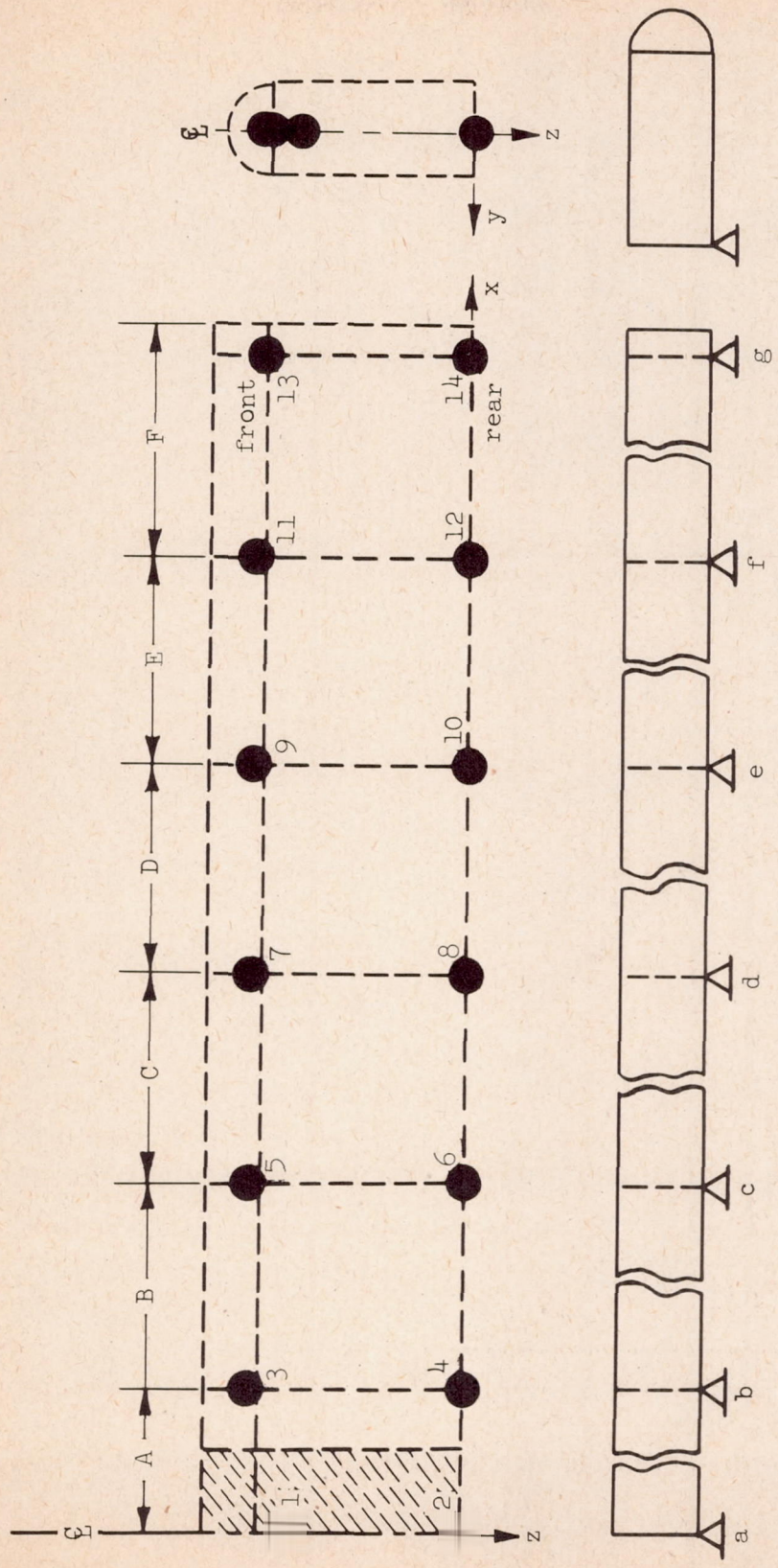

Figure 2.- Typical locations of masses replacing masses of actual structures.

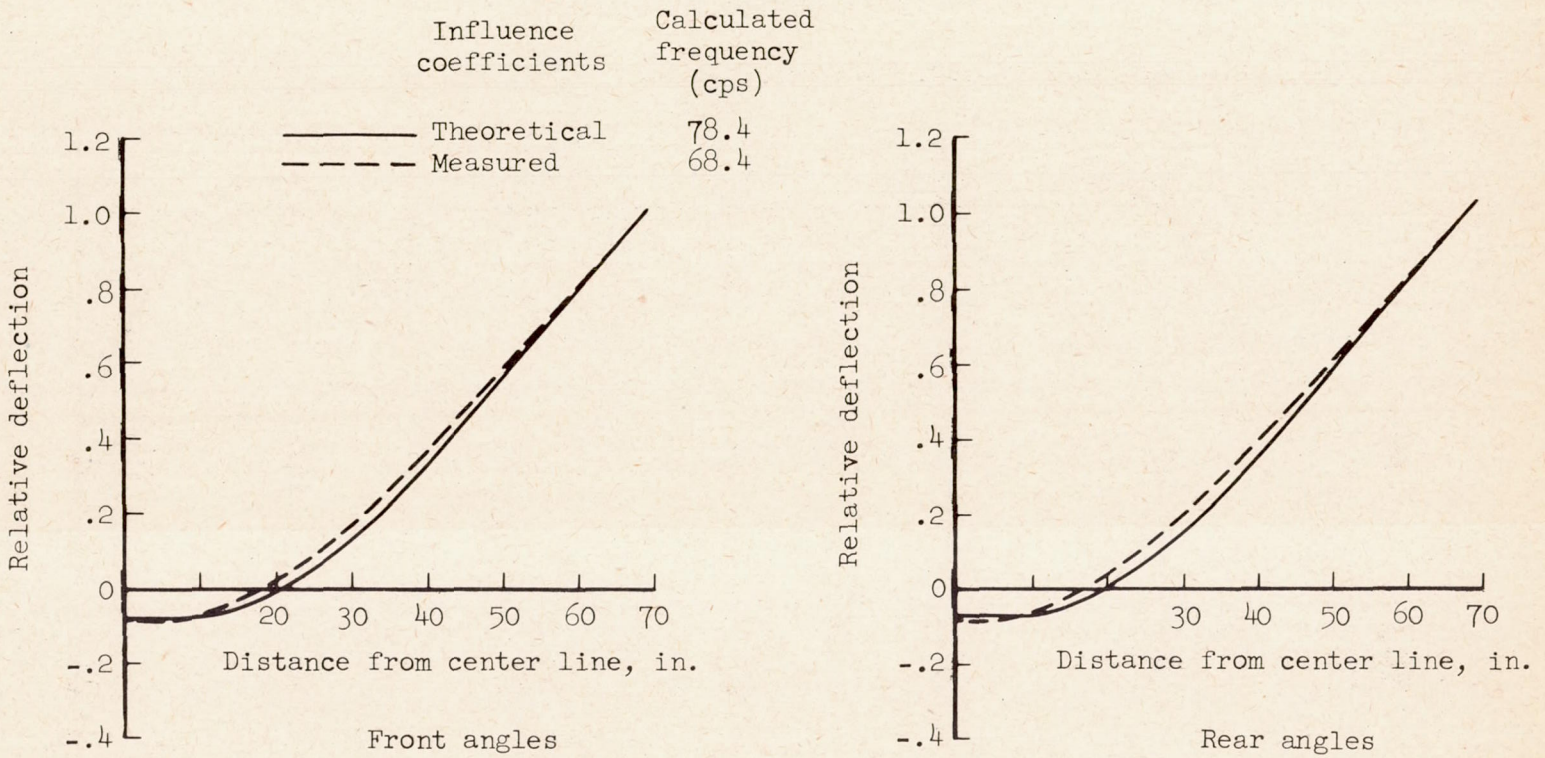

(a) Fundamental mode.

Figure 3.- Comparison of mode shapes of semibeam (specimen 1) calculated from both measured and theoretical influence coefficients.

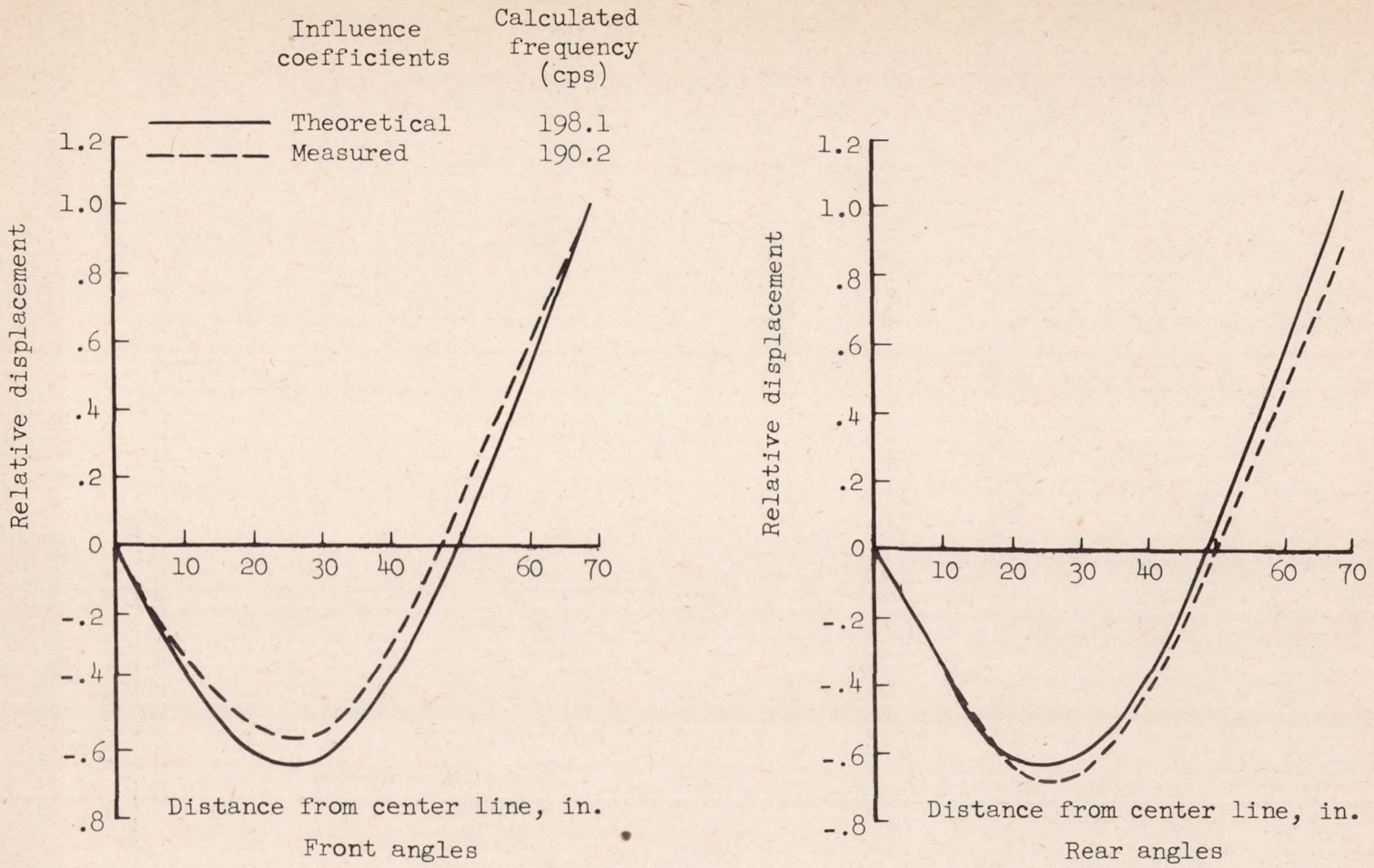

(b) Second resonance mode.

Figure 3.- Continued.

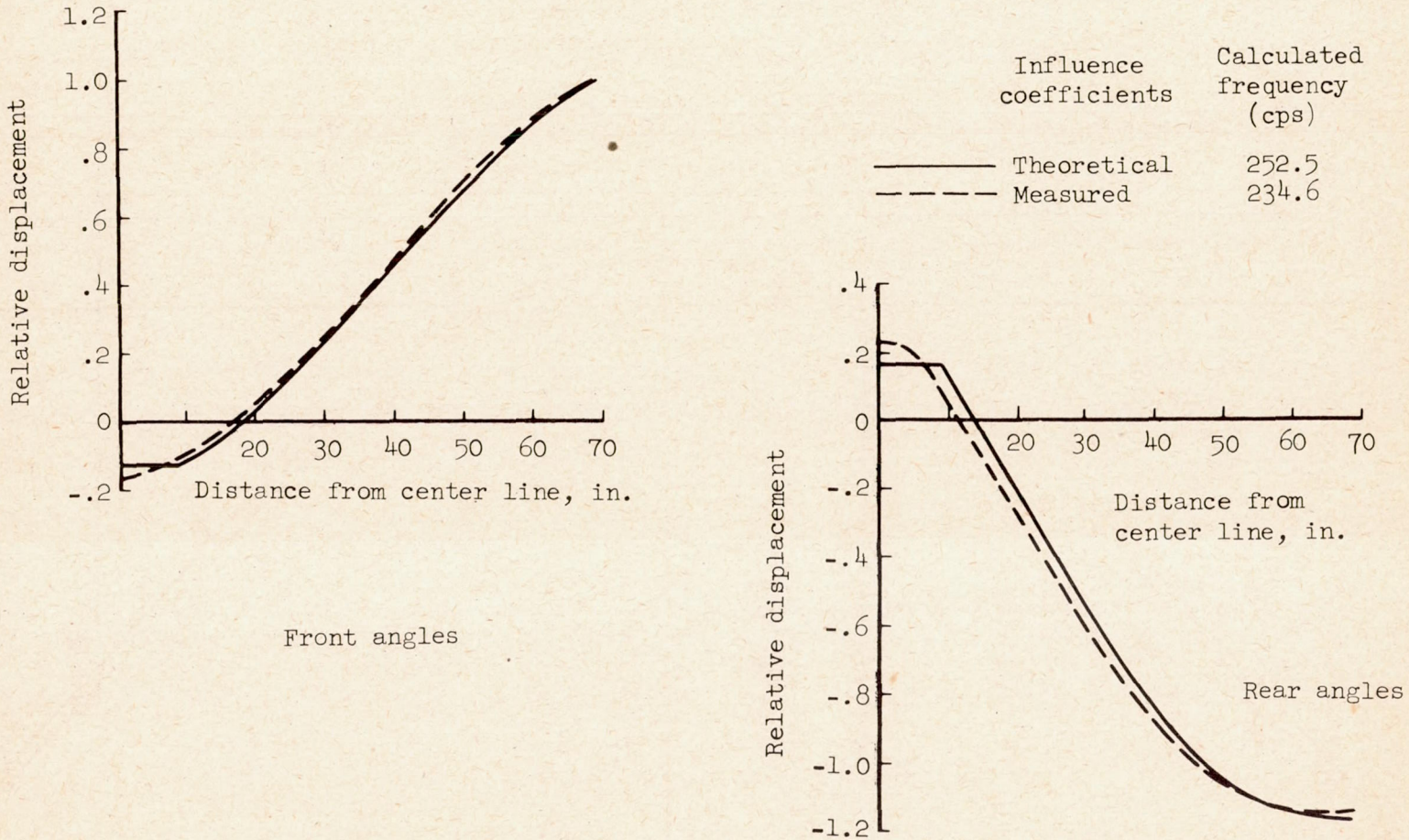

(c) Third resonance mode.

Figure 3.- Concluded.

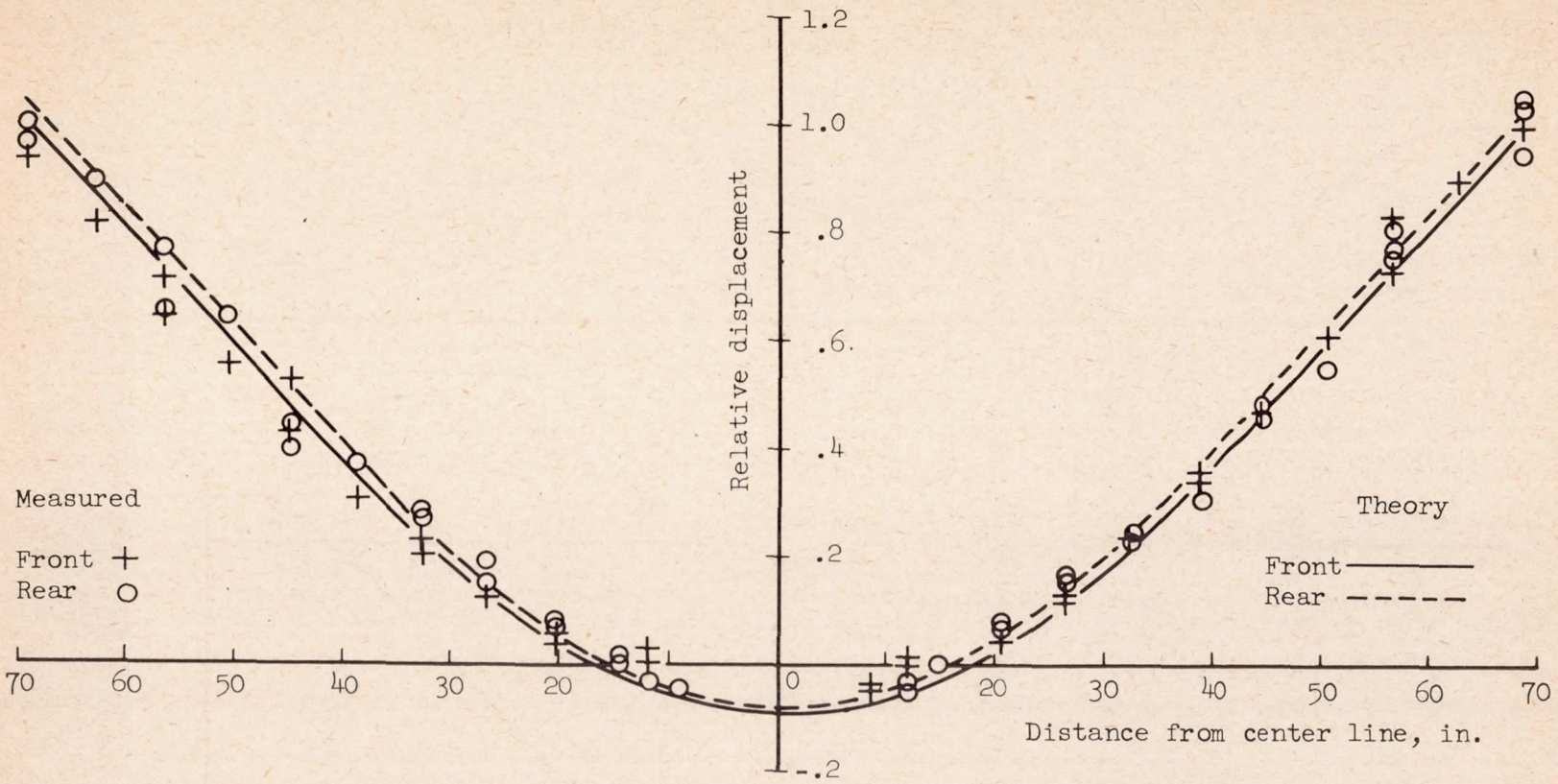

(a) Fundamental mode. Measured frequency, 66 cycles per second; calculated frequency, 68.4 cycles per second.

Figure 4.- Calculated and measured mode shapes of specimen 1. Calculated modes obtained from measured influence coefficients.

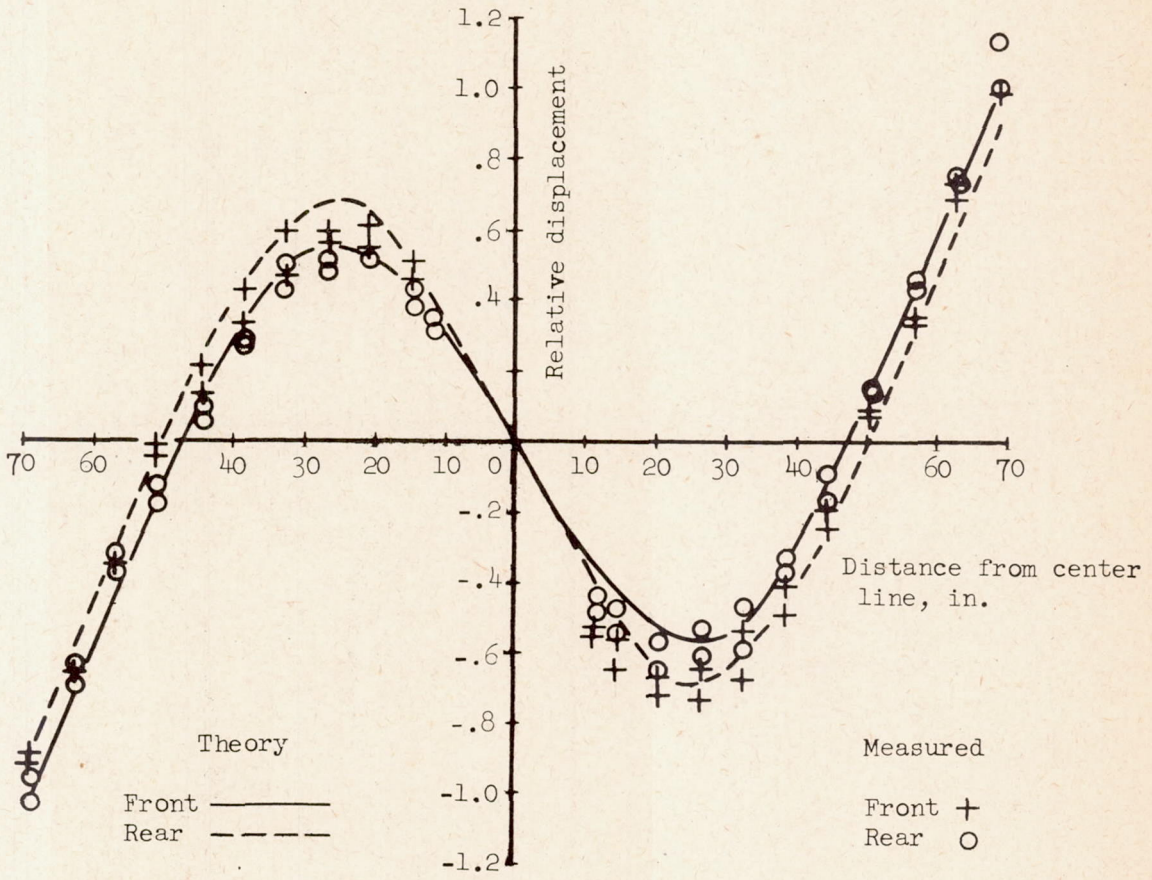

(b) Second resonance mode. Measured frequency, 181 cycles per second; calculated frequency, 190.2 cycles per second.

Figure 4.- Continued.

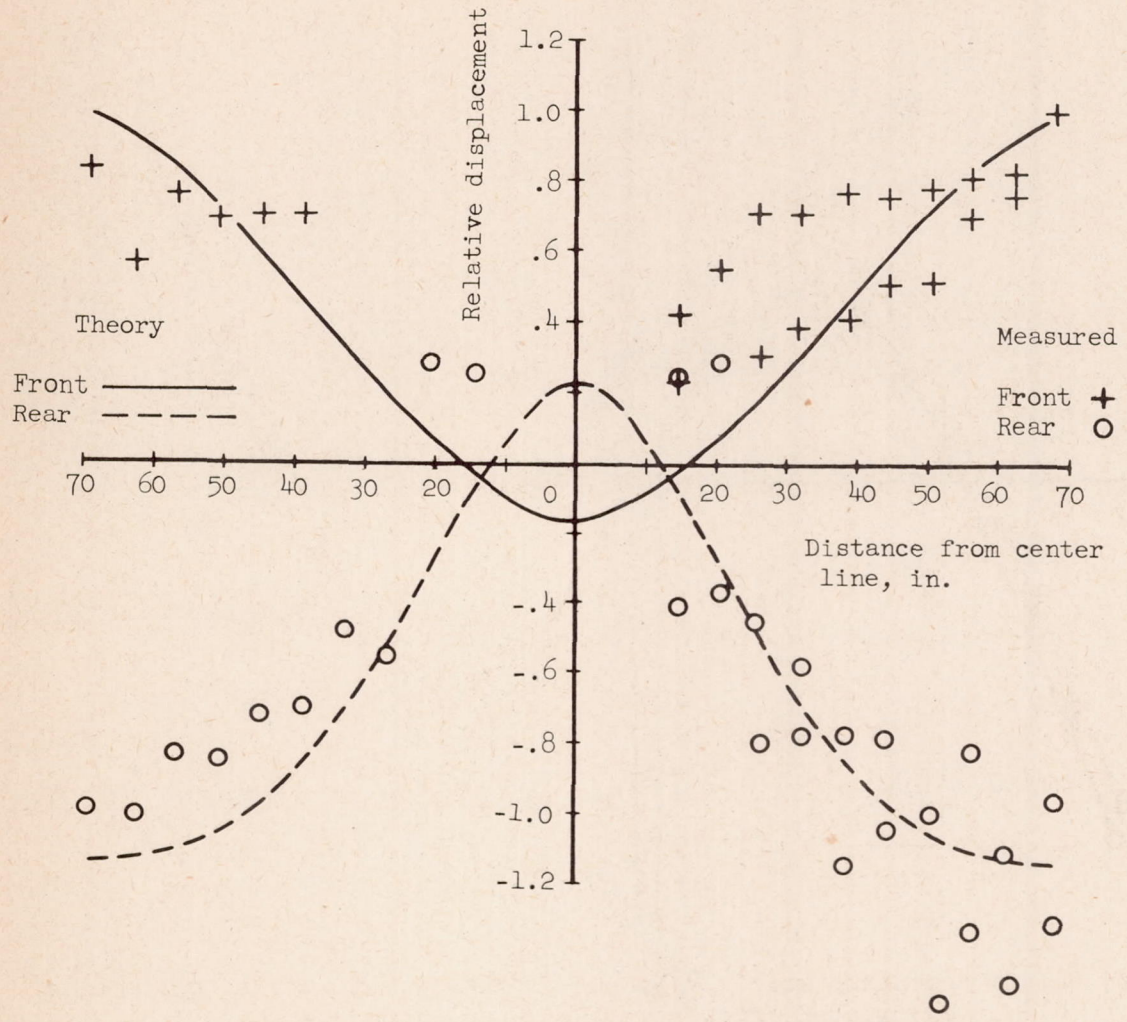

(c) Third resonance mode. Measured frequency, 221 cycles per second; calculated frequency, 234.6 cycles per second.

Figure 4.- Concluded.

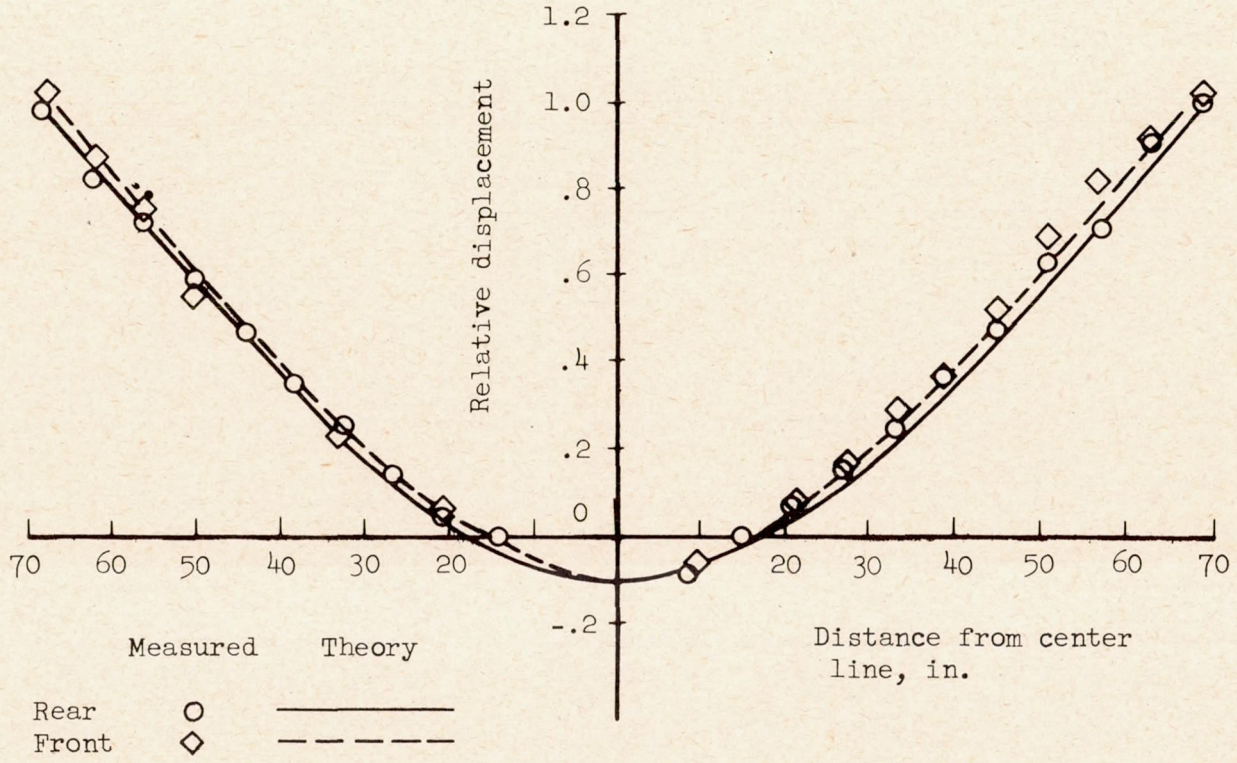

(a) Fundamental mode. Measured frequency, 63 cycles per second; calculated frequency, 64.8 cycles per second.

Figure 5.- Calculated and measured mode shapes of specimen 2. Calculated modes obtained from measured influence coefficients.

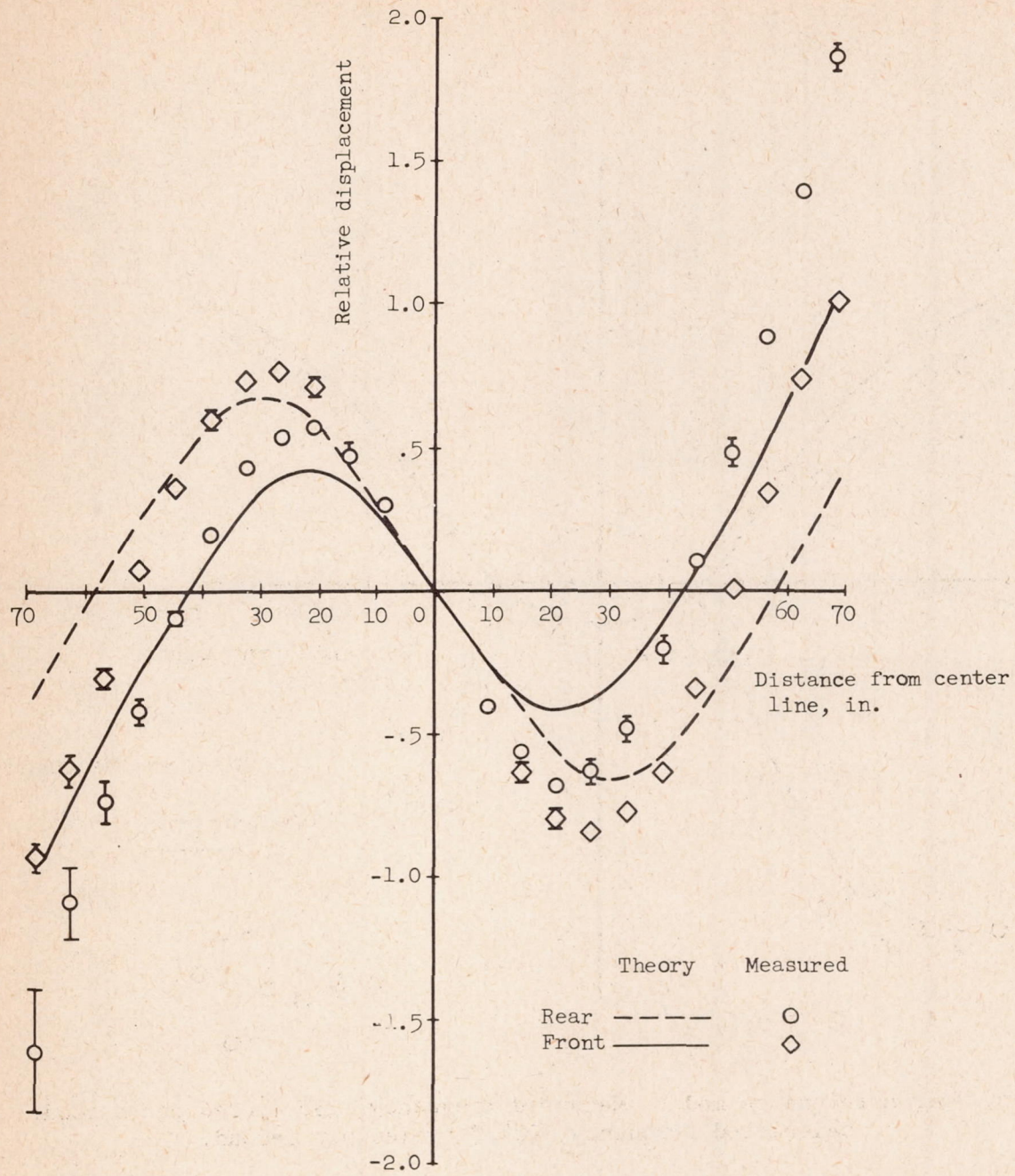

(b) Second resonance mode. Measured frequency, 173 cycles per second; calculated frequency, 181.3 cycles per second.

Figure 5.- Continued.

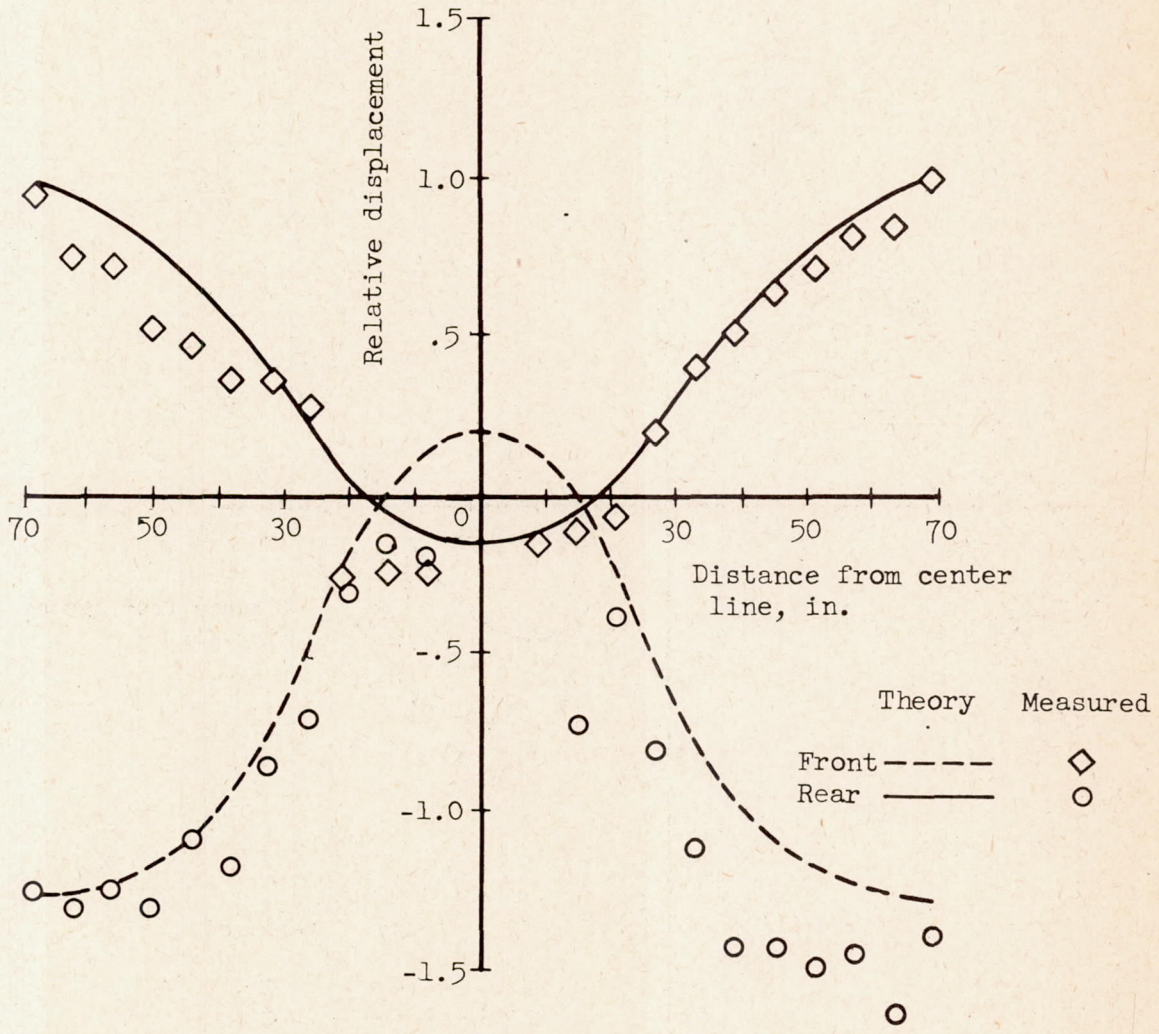

(c) Fourth resonance mode. Measured frequency, 198 cycles per second; calculated frequency, 204.7 cycles per second.

Figure 5.- Concluded.

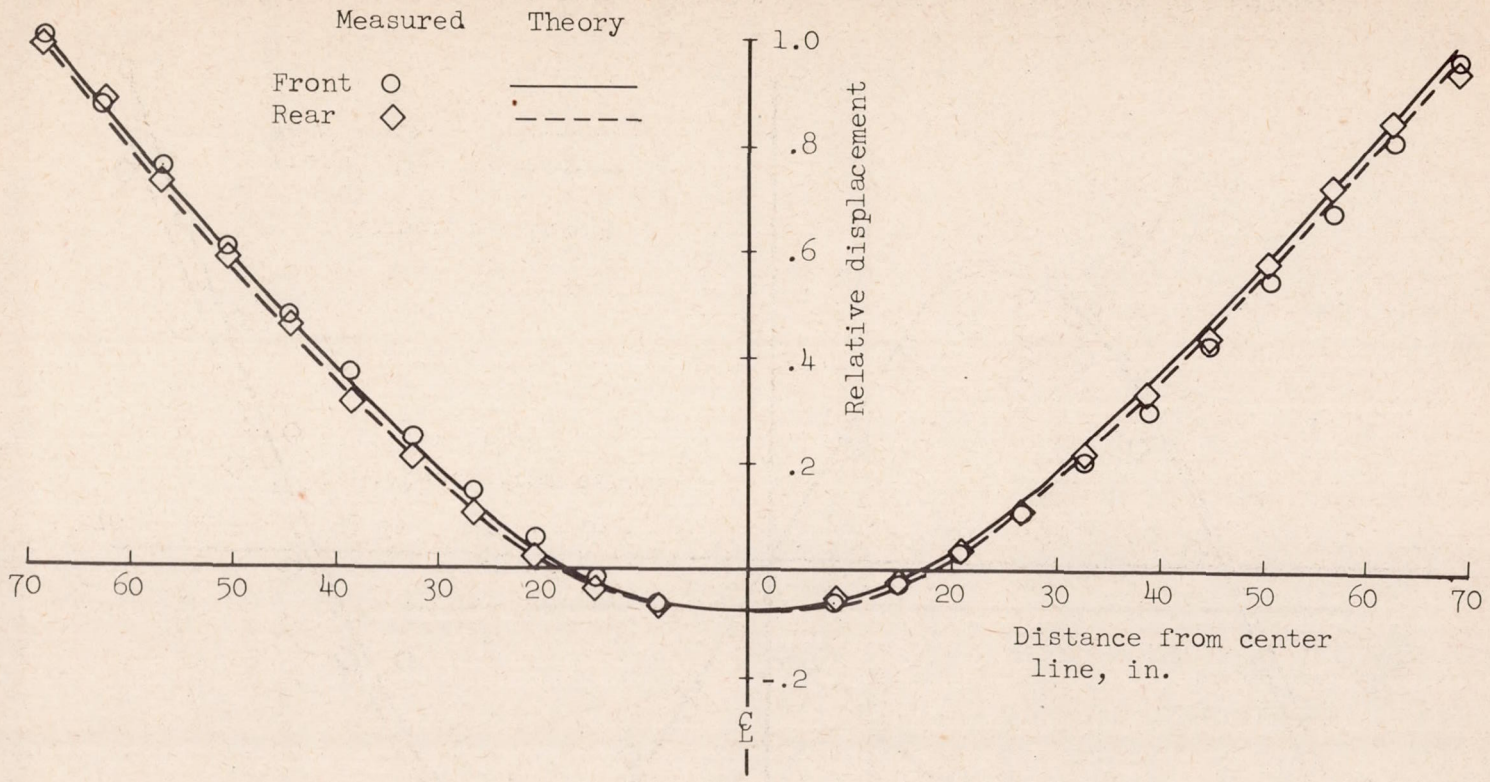

(a) Fundamental mode. Measured frequency, 64 cycles per second; calculated frequency, 66.3 cycles per second.

Figure 6.- Calculated and measured mode shapes of specimen 3. Calculated modes obtained from measured influence coefficients.

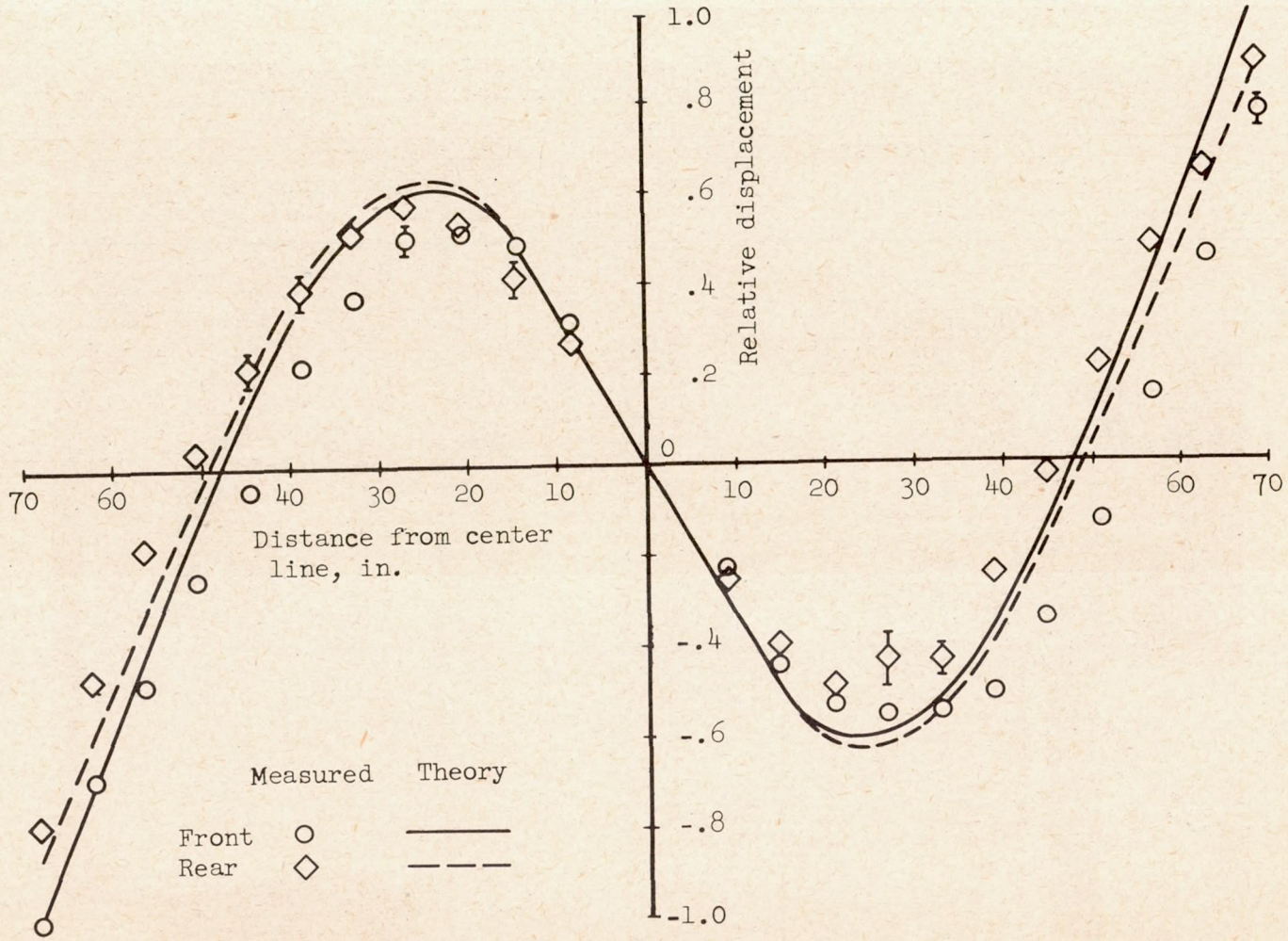

(b) Second resonance mode. Measured frequency, 173 cycles per second; calculated frequency, 179.5 cycles per second.

Figure 6.- Concluded.

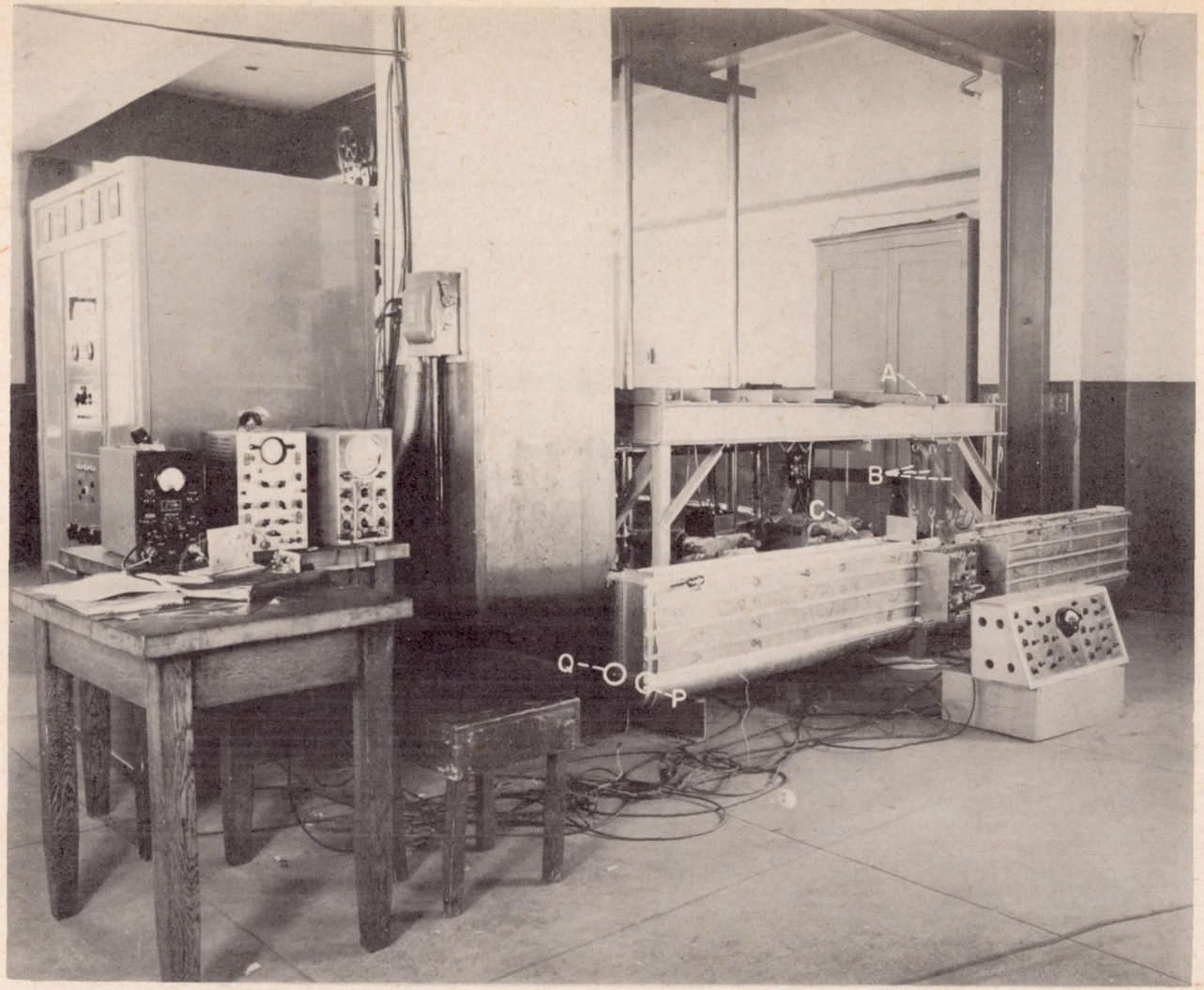

Figure 7.- Apparatus and specimen 2. Cantilevered channel, A; springs, B; pulsator, C; accelerometer stations, P and Q.

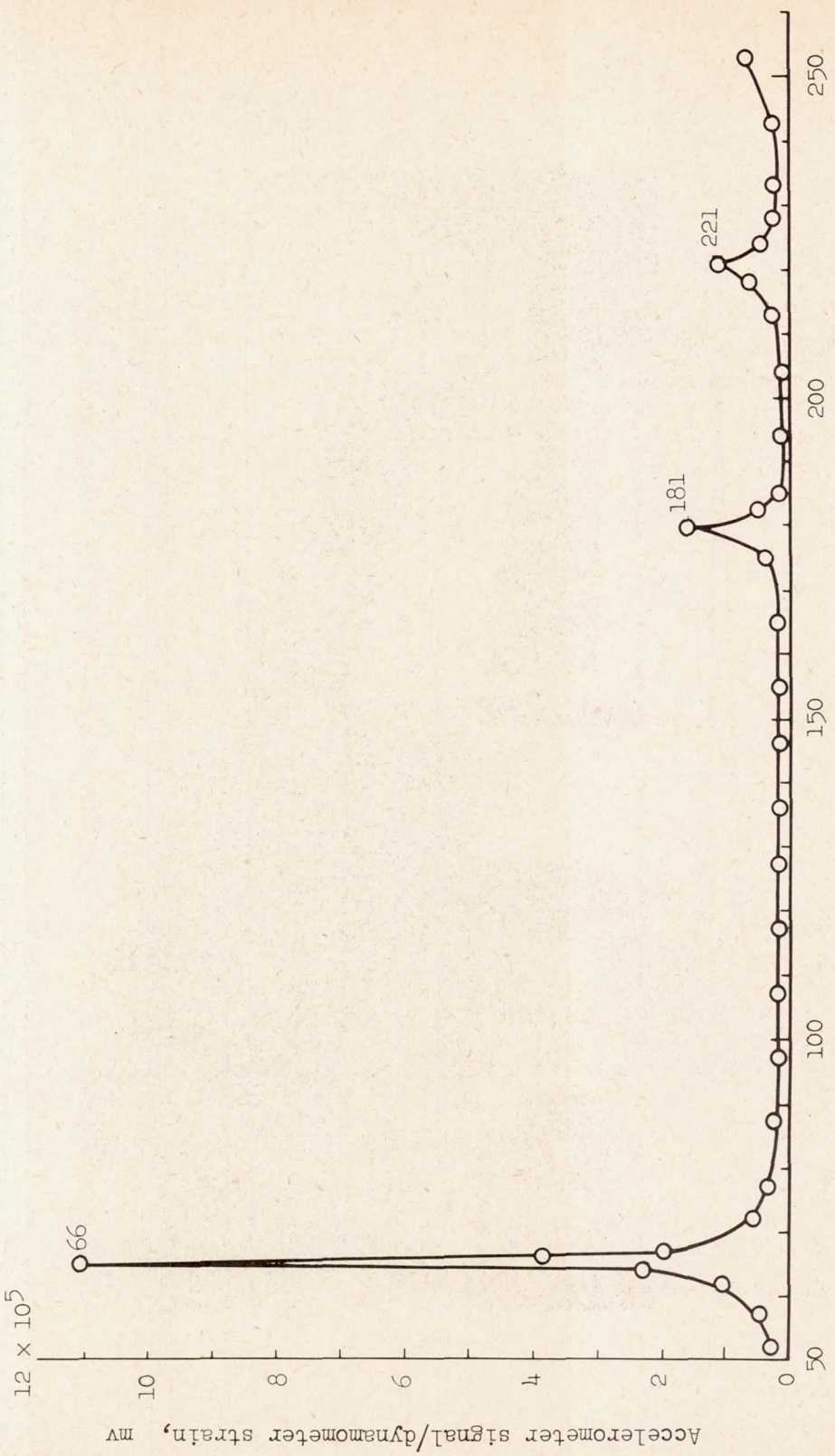

(a) Specimen 1.

Figure 8.- Resonance curves.

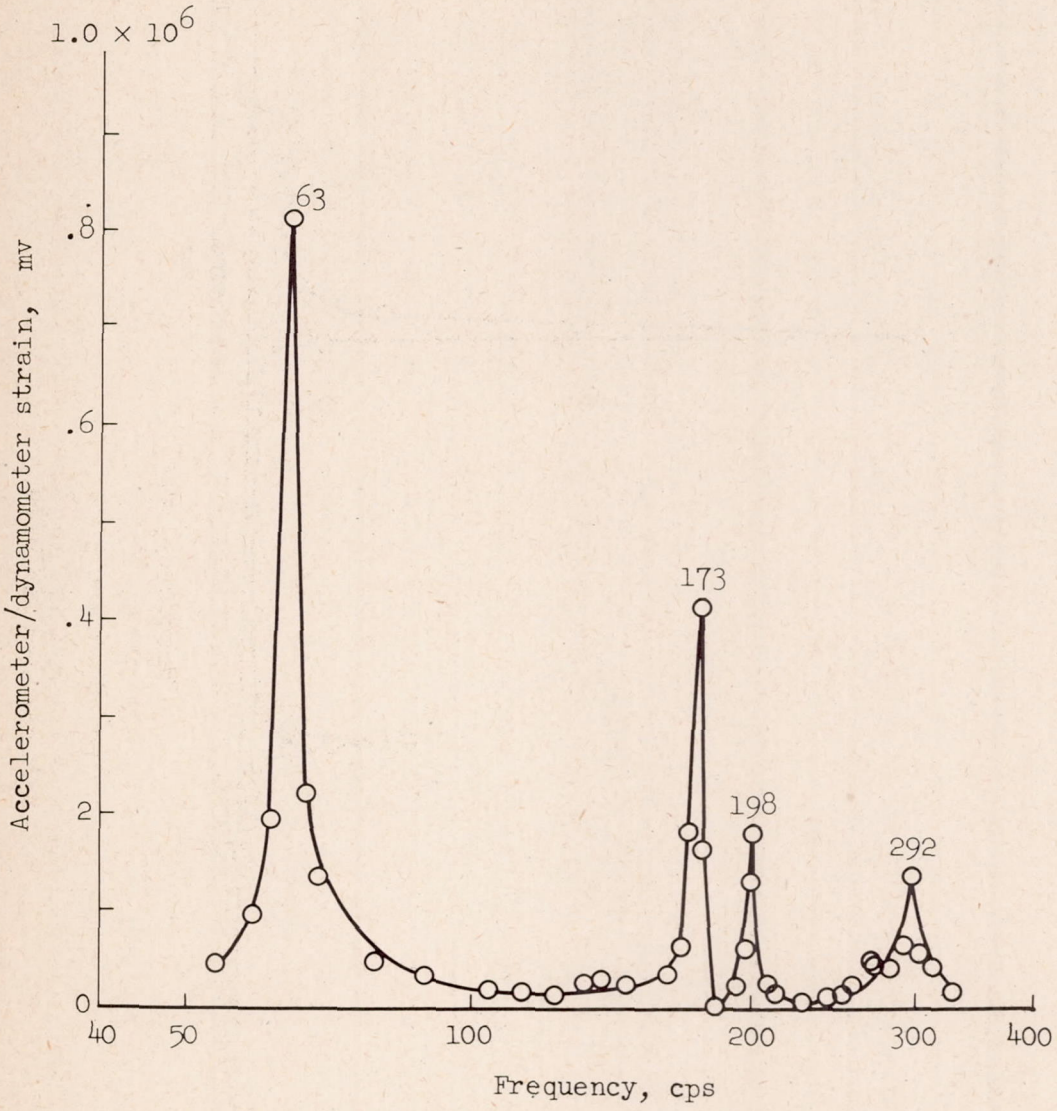

(b) Specimen 2.

Figure 8.- Continued.

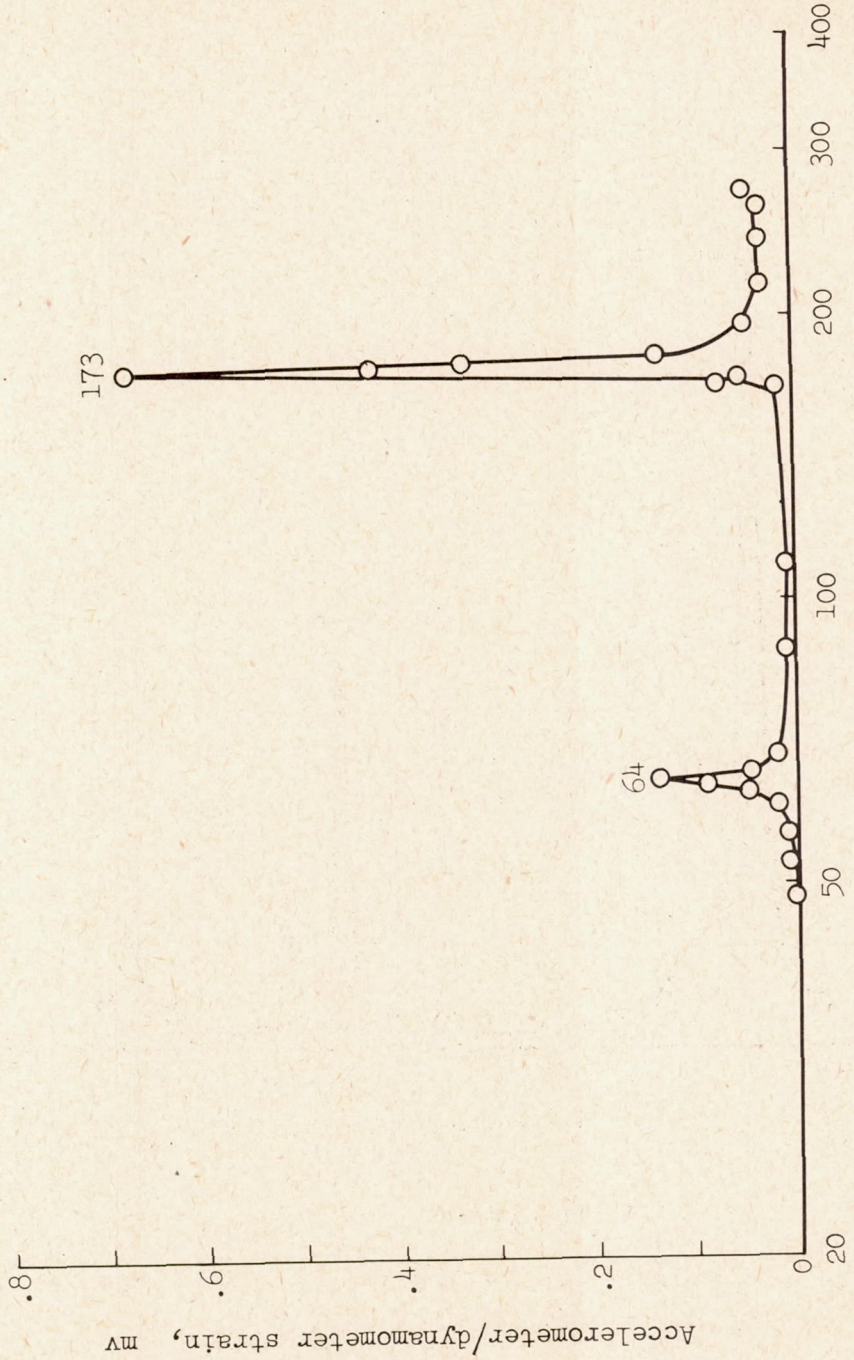

(c) Specimen 3.

Figure 8.- Concluded.